Zircon U–Pb ages and Hf isotope compositions of the Neoproterozoic magmatic rocks in the Helan Mountains, North China

Jie Yang[1,2] (iD), Qiang Zhu[1,3], Zuoxun Zeng[1,*] and Le Wan[1]

[1]School of Earth Sciences, China University of Geosciences, Wuhan 430074, PR China; [2]Changjiang Institute of Survey, Planning, Design, and Research, Wuhan 430010, PR China and [3]Geological Survey of Anhui Province, Hefei 23000, PR China

Abstract

The periodic dispersal and assembly of continental fragments has been an inherent feature of the continental crust. Based on the discovery of large-scale supercontinent cycle and the theory of plate tectonics, several supercontinents have been identified, such as Columbia/Nuna, Rodinia, Gondwana and Pangaea. Neoproterozoic magmatic events related to the break-up of Rodinia are globally well preserved. Although Neoproterozoic magmatic events were very weak in the North China Craton (NCC), they are crucial in reconstructing the geometries of the NCC and could facilitate the completion of the Neoproterozoic configuration of the supercontinent. In this study, *c.* 853–835 Ma magmatic rocks are identified in the western margin of the NCC. Precise zircon U–Pb age determination yields $^{206}Pb/^{238}U$ average ages of 835.5 ± 5.3 Ma (HL-39) and 853.7 ± 4.5 Ma (HL-30). *In situ* zircon Hf isotope compositions of the samples reveal that their parental magma was formed by the reworking of ancient crust evolved from Mesoproterozoic mantle. In summary, the discovery of Neoproterozoic magmatic rocks in the western margin of the NCC, and reported synchronous rocks in other parts of the NCC indicate that the NCC might be conjoined with the supercontinent Rodinia during the Neoproterozoic. This discovery is of significant help in unravelling the early Neoproterozoic history of the NCC and the evolution of the supercontinent Rodinia.

1. Introduction

The Neoproterozoic era was a tumultuous period in the history of the Earth, marked by the formation and break-up of the supercontinent Rodinia and the subsequent amalgamation of Gondwana (Merdith *et al.* 2017). Accompanied by the amalgamation and dispersal of the supercontinent, many aspects of the Earth system changed, such as the climate, rapid increase in oxygen, and emergence of complex life (e.g. Lyons *et al.* 2014; Cawood *et al.* 2016; Merdith *et al.* 2017). Neoproterozoic magmatic rocks, preserved in different continents, are thought to be tectonic markers of continental evolution (Halls *et al.* 2001; Hanski *et al.* 2006; Srivastava, 2010; Peng, 2015) and constraints on tectonic environments (Ernst *et al.* 2001). Matching the synchronous short-lived magmatic events from different continents and reconstructing their geometries could facilitate the completion of the Neoproterozoic configuration of the supercontinent (Peng, 2015). Those magmatic events associated with the assembly and break-up of Rodinia have been widely used to reconstruct the supercontinent (e.g. Yale & Carpenter, 1998; Greentree *et al.* 2006; Ernst *et al.* 2013; VH Isakson, unpub. data, 2017: http//:www).

The North China Craton (NCC), South China Craton (SCC) and Tarim Craton (TC) are three of the major Precambrian cratonic blocks in China (e.g. Zhao & Cawood, 2012; Zhao & Zhai, 2013; Wu *et al.* 2018) (Fig. 1a). Neoproterozoic magmatic events in TC (e.g. Shu *et al.* 2011; Xu *et al.* 2013; Zhang *et al.* 2013) and South China (e.g. Zhou et al. 2002; ZX Li *et al.* 2003; WX Li *et al.* 2005; Dong *et al.* 2011; Cui *et al.* 2015) indicate a relationship between the assembly and break-up of supercontinent Rodinia. However, owing to strong and multistage deformations and magmatism, as well as the extensive Mesozoic–Cenozoic sedimentation, geochronological records of Neoproterozoic magmatic activity in the NCC are very scarce. Therefore, the NCC has rarely been considered in the reconstruction of Rodinia (Liu *et al.* 2006).

In this study, *c.* 853–835 Ma magmatic rocks, named the Xiaosongshan complex, are identified in the western margin of the NCC. We analysed the zircon U–Pb dating results and the isotope compositions of Hf in the same zircon grains, using *in situ* analysis with a laser-ablation microprobe coupled to a multi-collector inductively coupled plasma mass spectrometer (MC-ICP-MS). These results in combination can reveal the relationship between the NCC and Rodinia. This discovery, along with the recently reported Neoproterozoic magmatic activity in the NCC and adjacent areas (e.g. R Peng *et al.* 2010; P Peng *et al.* 2011*b*; Wang *et al.*
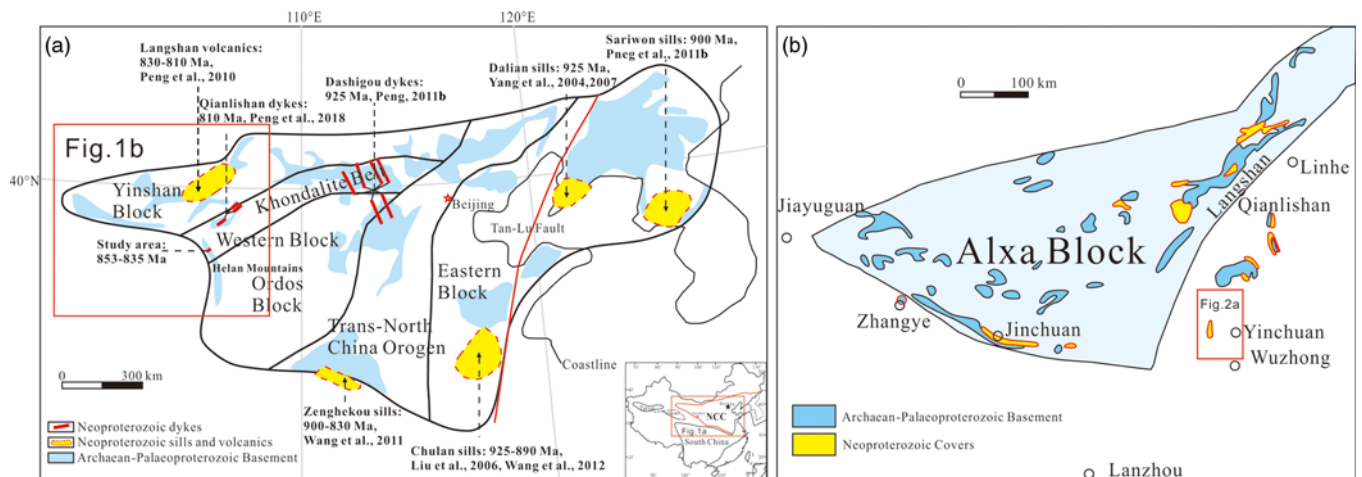
Fig. 1. (Colour online) Sketch map showing the distribution of Neoproterozoic mafic dyke swarms and tectonic subdivision of the NCC (a) and the Alxa Block (b) (modified from Zhao & Zhai, 2013; Peng, 2015; Peng et al. 2018).

2011; Peng, 2015; Zhang et al. 2016), contributes significantly to the understanding of the early Neoproterozoic history of the NCC and the evolution of Rodinia.

2. Geological background

2.a. Regional geology

The NCC is one of the oldest cratonic blocks in the world, covering over 300000 km^2 and containing rocks as old as c. 3.85 Ga (Liu et al. 1992; Song et al. 1996; Zhao & Zhai, 2013; Zhai, 2015). Traditionally, the NCC consists of the Precambrian basement and late Palaeoproterozoic–Palaeozoic sedimentary cover (Zhai, 2015). The Precambrian NCC can be further separated into the Archaean–Palaeoproterozoic metamorphic basement and the Palaeo-Mesoproterozoic unmetamorphosed cover, referred to as the Changcheng (1.8–1.6 Ga), Jixian (1.6–1.0 Ga) and Qingbaikou (1.0–0.8 Ga) groups (Lu et al. 2008; Zhao & Zhai, 2013). Because many basement rocks underwent intense deformation and widespread metamorphism during the Archaean to Palaeoproterozoic eons and were reworked during the Mesozoic to Cenozoic eras (e.g. Zhao & Cawood, 2012; Zhao & Zhai, 2013; Li et al. 2018; Wang et al. 2018), the Precambrian history of the NCC is complex and has remained poorly understood. Although the formation and tectonic evolution of the NCC are still not well understood, its origin and geological evolution can provide important insights into the amalgamation of the Earth and early Precambrian crustal accretion (Yin et al. 2011).

A number of collision models have been proposed regarding the tectonic subdivision of the NCC (e.g. Zhao et al. 2001; Kusky, 2011; Trap et al. 2011). Zhao et al. (2010) proposed that two terranes, separated by a continent–continent collisional belt, should be assigned to different continental blocks. Recognition of three Palaeoproterozoic orogenic belts (Zhao et al. 1998, 2001, 2005; Zhao & Zhai, 2013) – the Jiao–Liao–Ji Belt, Trans-North China Orogen and Khondalite Belt – revealed that the N–S-trending Trans-North China Orogen can divide the Precambrian basement of the NCC into eastern and western blocks (Fig. 1a), and the E–W-trending Khondalite Belt can further subdivide the Western Block into the Yinshan Block in the north and Ordos Block in the south. Ultimately, the amalgamation of the eastern and western

blocks at ∼1.85 Ga formed the NCC (Zhao et al. 2001, 2005; Zhang et al. 2006).

The N–S-trending Helan Mountains, whose range stretches 150 km long and 20–60 km wide, are located along the western margin of the NCC (Fig. 2a). The Archaean–Palaeoproterozoic metamorphic basement in this area consists mainly of the Helanshan (Archaean) and Zhaochigou complexes (Palaeoproterozoic), and the Palaeo-Mesoproterozoic cover is composed primarily of the Huangqikou Formation (Changcheng), Wangquankou Formation (Jixian) and Xihuashan complex (Qingbaikou). According to differences in geomorphological features, the Helan Mountains are usually divided into three portions from south to north. The study area lies within the northern portion of the Helan Mountains near the boundary between the Ordos Block and Khondalite Belt (Fig. 1a).

The studied magmatic rock, named the Xiaosongshan complex, is mostly distributed in the Xiaosongshan areas in the northern Helan Mountains near the boundary between Inner Mongolia and the Ningxia Hui Autonomous Region. The intrusions of magmatic rocks are spread out in the NW–SE direction, and their overall plane shapes cover ∼2.37 km^2, which can be presented as an isosceles triangle c. 4 km long (Fig. 2b, c). According to the 1:200000 Jilantai regional geological survey performed by the Ningxia Hui Autonomous Region Monitoring Institute of Land and Resources Survey (NXMILRS), the Xiaosongshan complex was assumed to be formed in the middle–late Devonian (K/Ar ages of ∼384.4 Ma) (Wang et al. 2008). However, the age data from Wang et al. (2008) are sparse and have low precision, and higher-precision data have not been reported. Thus, the age of the Xiaosongshan complex is still a matter of controversy. In this study, we carried out a detailed petrological, geochronological and geochemical analysis of the Xiaosongshan complex with the goal of elucidating its precise age and origin.

2.b. Sample descriptions

The Xiaosongshan complex is surrounded by sedimentary and metamorphic rocks, including carbonatites from the Cambrian–Ordovician Abuchehe and Majiagou formations in the west and southwest, clastic rocks from the Jurassic Anding formation in the southeast, and gneisses from the Archaean Zongbieli complex
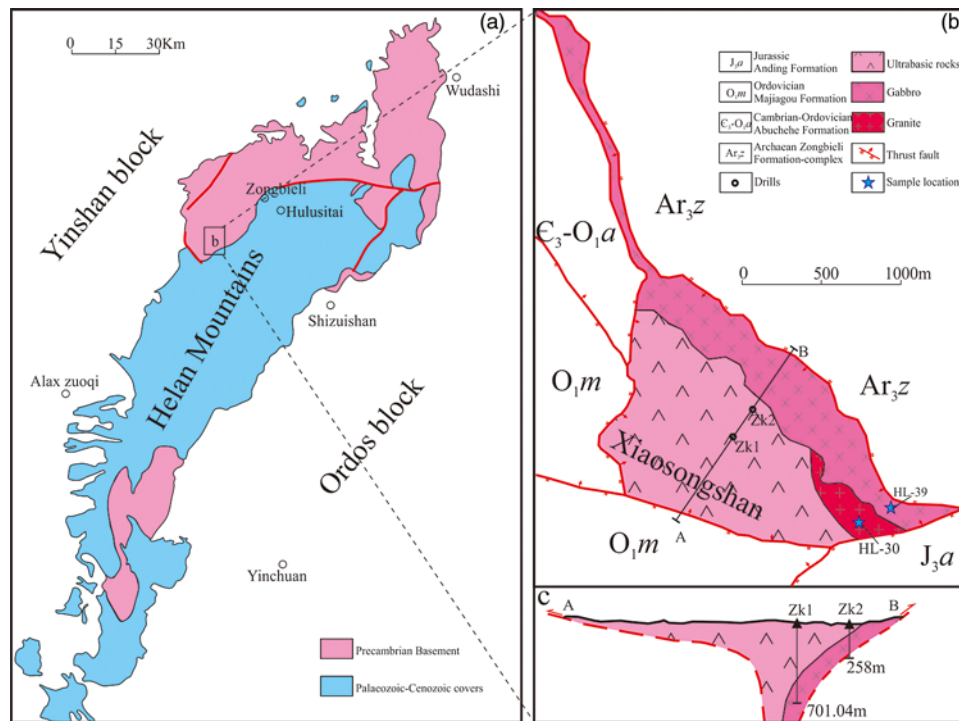
Fig. 2. (Colour online) Geological sketch map of the Helan Mountains (a) and the Xiaosongshan complex (b) (modified from Wang *et al*. 2008; D. Li *et al*. 2018). (c) A cross-section from SW to NE of the magmatic rocks in the study area. Section and drill numbers match those in (b). (Drilling data are from Zhao, 2003.)

in the northeast (Fig. 2b). There is significant thrust fault contact between the magma intrusions and the surrounding rocks, as well as some thermal contact metamorphic features (Wang *et al*. 2008). In the studied area, the Xiaosongshan complex is composed of ultrabasic rocks, gabbros and granites.

The ultrabasic rocks are composed primarily of olivine, diopside and plagioclase, with accessory minerals of spinel, apatite and ilmenite. Under the microscope, the granite sample consists of plagioclase (50–55 vol. %), microcline (10–15 vol. %), quartz (~20 vol. %), biotite (~8 vol. %) and minor accessory minerals (~2 vol. %) such as magnetite, apatite and sphene (Fig. 3). The gabbro sample contains plagioclase (45–55 vol. %) and pyroxene (40–50 vol. %), with small amounts of biotite, hornblende and magnetite.

3. Materials and methods

Two representative samples (HL-39 and HL-30) were collected from the Xiaosongshan complex in the northern Helan Mountains for the zircon U–Pb and Hf isotope analysis (Fig. 2b). Gabbro sample HL-39 (location: 39° 06′ 17″ N, 106° 02′ 06″ E) was obtained from the eastern part of the Xiaosongshan complex. Granite sample HL-30 (location: 39° 06′ 31″ N, 106° 02′ 16″ E) was collected from the southeastern part of the Xiaosongshan complex. Thin-sections of the samples were prepared for microscopic observation.

The samples were cleaned using nanopore deionized water, and the weathered surface was removed. The fresh and unaltered samples were then processed for heavy-mineral, liquid and magnetic separation. Zircon particles from non-magnetic fractions were selected under the binocular microscope at the Langfang Integrity Geological Services Incorporation (LFIGSI). The zircons were polished and photographed in reflected light and transmitted light, and through backscattered scanning electron (BSE)

microscopy and cathodoluminescence (CL) using the JXA-8100 electron probe. Zircon system analysis, microscopic imaging and zircon U–Pb dating were carried out in the State Key Laboratory of Geological Processes and Mineral Resources, China University of Geosciences. Zircon U–Pb dating was performed using the Agilent 7700a ICP-MS instrument, equipped with the 193-nm GeoLas 2005. The adopted laser diameter was 32 μm. Helium and argon were applied as the carrier gas and compensation gas. Detailed analytical methods were described by Li *et al*. (2014). Errors of a single data point were quoted at the 1σ level, and the errors of the weighted average age were quoted at the 2σ (95%) confidence level. Zircon U–Pb dating data are presented in Supplementary Tables 1 and 2.

In situ zircon Hf isotope analysis was conducted at the State Key Laboratory of Geological Processes and Mineral Resources, China University of Geosciences, using a Neptune Plus MC-ICP-MS (Thermo Fisher Scientific, Germany) in conjunction with a GeoLas 2005 excimer ArF laser ablation system (Lambda Physik, Göttingen, Germany). Detailed analytical methods were the same as outlined by Hu *et al*. (2008*a*, *b*). The results of the zircon Hf isotope compositions for the samples are listed in Supplementary Tables 3 and 4.

4. Results

4.a. Zircon U–Pb geochronology

A total of 18 zircon grains were selected from the gabbro sample (HL-39), and 20 analysis points distributed among them were selected for zircon U–Pb dating. Based on the photomicrographs and CL images obtained (Fig. 4), the zircon crystals display oscillatory zoning without any inheritable cores or metamorphic rims. The CL images, as well as the relatively high concentrations of Th
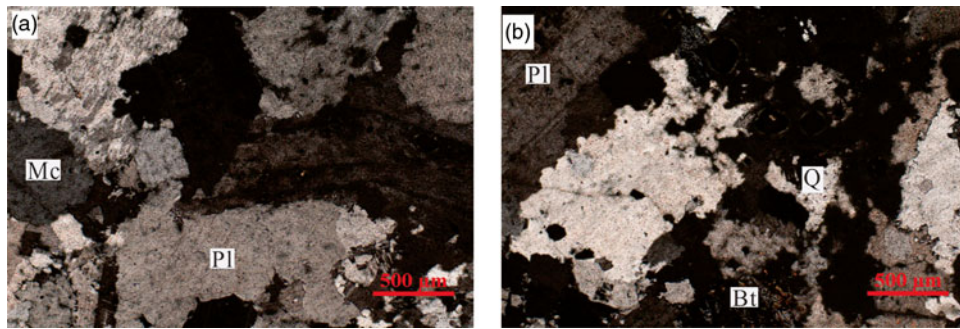
Fig. 3. (Colour online) Microphotographs for the biotite monzogranite samples (a, b) Pl. plagioclase; Mc. microcline; Bt. Biotite; Q. quartz.
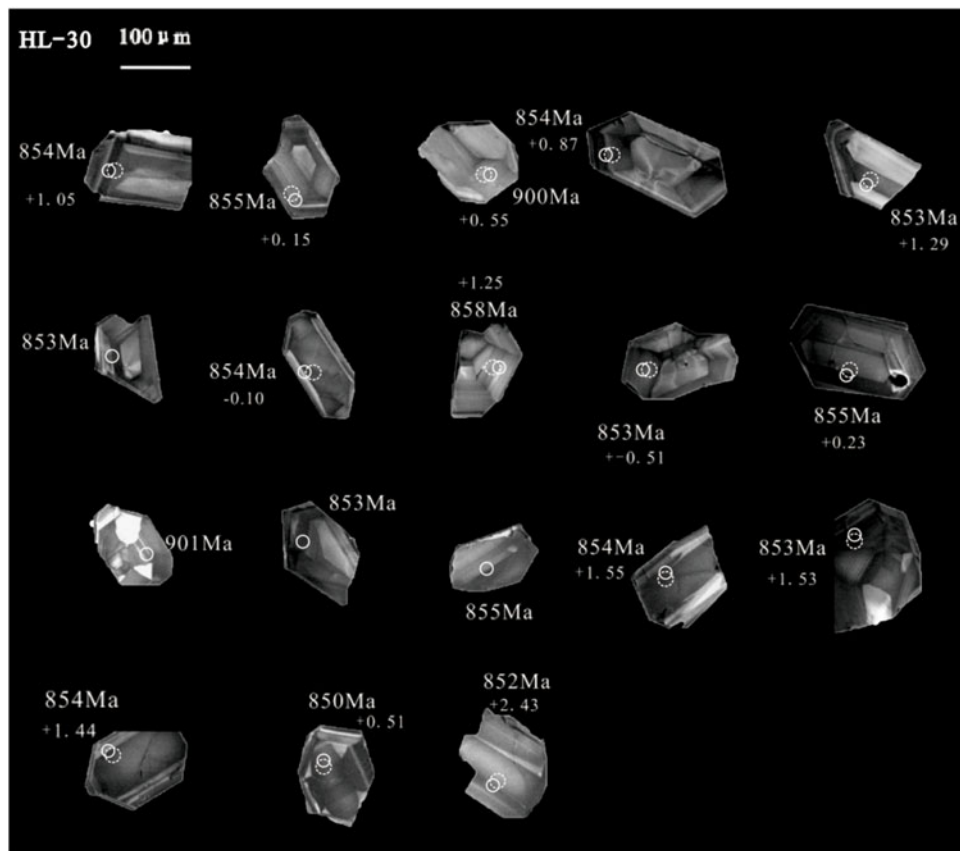

Fig. 4. CL images of representative magmatic zircon crystals from the granite (HL-30). Morphology of zircon grains, $\varepsilon Hf(t)$ values (large broken white line circles) and $^{206}Pb/^{238}U$ ages (small white circles) are presented.

and U (ranging from 20×10^{-6} to 113×10^{-6} and from 44×10^{-6} to 182×10^{-6}, respectively) and Th/U ratios (ranging from 0.38 to 0.67) (Supplementary Table 1), indicate a magmatic origin (Wu & Zheng, 2004). Zircon U–Pb dating results for the gabbro (HL-39) are listed in Supplementary Table 1 and on the concordia U–Pb age diagrams (Fig. 5). The $^{206}Pb/^{238}U$ ages for the gabbro vary from 833 ± 11 Ma to 840 ± 16 Ma, with an average age of 835.5 ± 5.3 Ma ($n = 20$, mean square weighted deviation (MSWD) = 0.035).

Likewise, 18 zircon grains were selected from the granite sample and 18 analysis points distributed among them were selected for zircon U–Pb dating. It can be seen from the CL images that these grains mostly show good crystal, euhedral–subhedral, short column–

rhombohedron morphology and wide oscillatory zones, indicating a magmatic origin. The concentrations of Th and U in samples are from 64×10^{-6} to 488×10^{-6} and from 180×10^{-6} to 674×10^{-6}, respectively, with Th/U ratios ranging from 0.35 to 0.75 (Supplementary Table 2). These relatively high concentrations of Th and U and Th/U ratios reveal a magmatic origin (Wu & Zheng, 2004). Zircon U–Pb dating results for the granite sample (HL-30) are listed in Supplementary Table 2 and on the concordia U–Pb age diagrams (Fig. 5). The granite $^{206}Pb/^{238}U$ ages vary from 850 Ma to 860 Ma (except two inheritable magmatic zircons with ages of 900 Ma and 901 Ma), with an average age of 853.7 ± 4.5 Ma ($n = 16$, MSWD = 0.028).
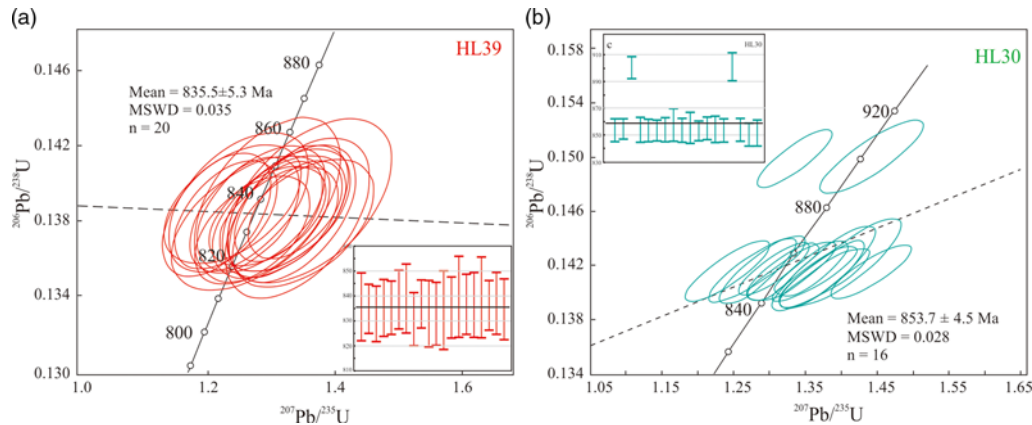
Fig. 5. (Colour online) Concordia U–Pb age diagrams and average U-Pb age plots for the gabbro sample HL-39 (a) and granite sample HL-30 (b).

4.b. Zircon Hf isotope compositions

In situ zircon Hf isotope compositions for the samples are presented in Supplementary Tables 3 and 4. The εHf(*t*) values and Hf model ages (*T*$_{DM}$) were calculated using

$$\varepsilon Hf(t) = \{[(^{176}Hf/^{177}Hf)_S - (^{176}Lu/^{177}Hf)_S \\ \times (e^{\lambda t} - 1)]/[(^{176}Hf/^{177}Hf)_{CHUR,0} - (^{176}Lu/^{177}Hf)_{CHUR} \\ \times (e^{\lambda t} - 1)] - 1\} \times 10000,$$

(1)

$$T_{DM} = 1/\text{lln}\{1 + [(^{176}Hf/^{177}Hf)_S - (^{176}Hf/^{177}Hf)_{DM}] \\ /[(^{176}Lu/^{177}Hf)_S - (^{176}Lu/^{177}Hf)_{DM}]\}.$$

(2)

To calculate the εHf(*t*) values, we use the ^{176}Lu decay constant of λ = 1.865 × 10^{-11} a^{-1} (Scherer *et al.* 2001) and the chondritic values of ^{176}Lu/^{177}Hf = 0.0336 and ^{176}Hf/^{177}Hf = 0.28275 (Bouvier *et al.* 2008). The depleted mantle values of ^{176}Lu/^{177}Hf = 0.0384 (Griffin *et al.* 2000) and ^{176}Hf/^{177}Hf = 0.28325 (Nowell *et al.* 1998), and the average mafic lower continental crust values of ^{176}Lu/^{177}Hf = 0.34 were used to calculate the two-stage model ages (*T*$_{DM2}$).

A total of 15 analysis points distributed among 13 zircon grains in sample HL-39 were selected for the zircon Hf isotope composition analysis using laser ablation (LA-)MC-ICP-MS. The ^{176}Yb/^{177}Hf ratios and the ^{176}Hf/^{177}Hf ratios of sample HL-39 vary from 0.012570 to 0.034272 and from 0.282421 to 0.282478, respectively (Supplementary Table 3). The initial εHf(*t*) values of the zircons with an age of ∼835 Ma range from 5.83 to 7.87. The Hf single-stage model ages (*T*$_{DM1}$) and Hf two-stage model ages (*T*$_{DM2}$) range from 1075 Ma to 1155 Ma and from 1176 Ma to 1289 Ma, respectively (Supplementary Table 3).

In addition, 14 analysis points distributed among 14 zircon grains in the granite sample HL-30 were selected for the zircon Hf isotope composition analysis using the same method. The ^{176}Yb/^{177}Hf ratios and ^{176}Hf/^{177}Hf ratios vary from 0.034849 to 0.187297 and from 0.000806 to 0.003991, respectively (Supplementary Table 4). The εHf(*t*) values are between −0.51 and 2.43, and the corresponding *T*$_{DM1}$ and *T*$_{DM2}$ ages vary from 1348 Ma to 1461 Ma and from 1493 Ma to 1655 Ma, respectively (Supplementary Table 4).

5. Discussion

5.a. Formation ages of the Xiaosongshan complex

The formation age of the Xiaosongshan complex has long remained uncertain owing to the lack of isotopic age data. As discussed above, based on the K–Ar isotopic age of olivine from the basic–ultrabasic complex rocks, the Xiaosongshan complex has been interpreted to be formed during the middle–late Devonian (Wang *et al.* 2008). However, because of low precision and sparse data points, these ages are disputable. Higher-precision data are needed to constrain the formation age of these magmatic rocks. In this study, the zircon U–Pb ages of the gabbro and granite samples provide new geochronological constraints on the Xiaosongshan complex.

The majority of zircons in the gabbro sample (HL-39) are euhedral–subhedral with fine-scale oscillatory zoning and relatively high Th/U ratios (0.38–0.67), indicating a magmatic origin. Furthermore, no inheritable or captured zircons were observed for the zircon CL images. Thus, the average ^{206}Pb/^{238}U age of 835.5 ± 5.3 Ma for zircon in the gabbro sample (HL-39) should represent the crystalline age of the gabbro intrusion.

Likewise, the characteristics of the zircon in the granite sample (HL-30) and the relatively high Th/U ratios (0.35–0.75) indicate a magmatic origin. Two analysis points (HL-30-3 and HL-30-15) yield relatively older ages (^{206}Pb/^{238}U ages of 900 Ma and 901 Ma, respectively) than the other 16 analysis points (average ^{206}Pb/^{238}U age of 853.7 ± 4.5 Ma). Based on similar observations regarding magmatic rocks and basement of the Alxa Block and the western NCC, Peng *et al.* (2018) suggested that the Alxa Block was a part of the NCC during the Neoproterozoic. Furthermore, the U–Pb age and Hf isotope features of detrital zircons indicate that the Helan Mountains had received clastics from the Alxa Block in the Neoproterozoic (Dong *et al.* 2017). Therefore, based on the early Neoproterozoic (∼900 Ma) magmatic event in the Alxa area of Inner Mongolia on the western margin of the NCC (Geng & Zhou, 2010, 2011), we interpret the two ∼900 Ma zircons to be inheritable magmatic zircons. The average ^{206}Pb/^{238}U age of 853.7 ± 4.5 Ma from the other 16 analysis points, therefore, represents the crystalline age of the granite intrusion, indicating the granites (*c.* 853 Ma) and the gabbros (*c.* 835 Ma) are contemporaneous.
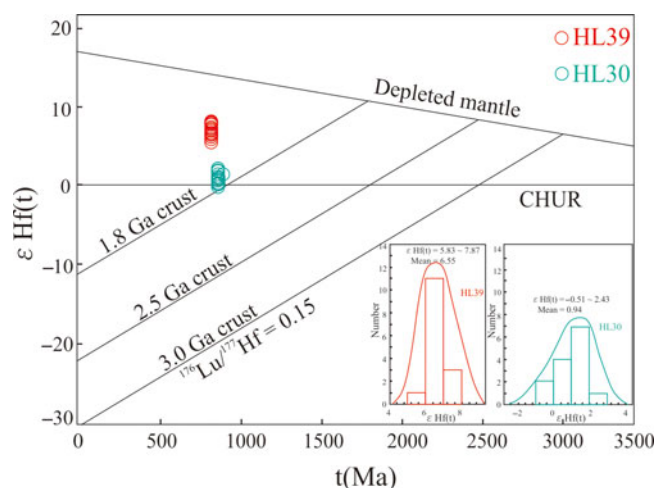
Fig. 6. (Colour online) Zircon formation age vs. zircon εHf(t) diagrams and Histograms of the zircon εHf(t) for the gabbro sample HL-39 and granite sample HL-30.

5.b. Implication of the zircon Hf isotope results

As a common accessory mineral in most rocks, zircon typically contains 0.5–2 wt % Hf in its crystal structure and its $^{176}Lu/$ ^{177}Hf ratio is extremely low (usually less than 0.002). The ^{176}Hf that comes from the beta decay of ^{176}Lu is negligible. The $^{176}Lu/^{177}Hf$ ratios in zircon are regarded as the initial values at the time of its formation (Hu *et al.* 2012). Therefore, the isotope compositions of Hf in zircon can provide relevant information for deciphering the origin of zircon grains (Patchett *et al.* 1982; Knudsen *et al.* 2001; Wu *et al.* 2007) and the evolution of the crust (Cherniak *et al.* 1997; Hawkesworth & Kemp, 2006).

We analysed the zircon Hf isotope composition with the LA-MC-ICP-MS method, together with the U–Pb age dating for the same zircon grain. The $^{176}Lu/^{177}Hf$ ratios of the gabbro (HL-39) and the granite (HL-30) vary from 0.0002 to 0.0007 and from 0.0008 to 0.003, respectively (Supplementary Table 3). Moreover, the concentration of Lu is extremely low, indicating that the ^{176}Hf, which came from the decay of ^{176}Lu, is negligible. This corroborates that the $^{176}Lu/^{177}Hf$ ratios in zircon can represent the initial values of the zircon (Hu *et al.* 2012).

The zircon Hf isotope compositions of the gabbro (HL-39) are relatively high (with εHf(t) of 5.83–7.87). The plotted points in the zircon formation age vs zircon εHf(t) diagrams are primarily located between the trends representing the chondrite and the evolutionary trends of the depleted mantle, near the evolutionary trends of the *c.* 1.8 Ga crustal rocks (Fig. 6). This suggests a similar genesis for these zircons and an older mantle origin for the protoliths. If the Hf model ages exceed the formation ages of zircons, the parent rocks should remain in the crust for a period of time, and the two-stage Hf model age may reflect the extraction time of the protoliths from the mantle (Wu et al. 2007; Geng *et al.* 2012). These zircons are younger, with their mean U–Pb ages being 835.5 ± 5.3 Ma, as compared to those determined by the Hf single-stage model (T_{DM1}) and Hf two-stage model (T_{DM2}); the models determined their ranges to be 1075–1155 Ma and 1176–1289 Ma, respectively. These observations suggest that the parent rocks, which are derived from the Mesoproterozoic mantle, must have remained settled in the crust for a period of time to be modified along with the ancient crustal rocks.

The εHf(t) values of the granite (HL-30) range between −0.51 and 2.43 (mean = 0.94), and remain close to 0. In the zircon

formation age vs zircon εHf(t) diagrams, the plotted points are mainly located near the chondrite (Fig. 6), implying that the source materials of the granite were produced by the partial melting of the crustal rocks. Because the corresponding Hf single-stage model ages (T_{DM1}) and Hf two-stage model ages (T_{DM2}) (varying from 1348 Ma to 1461 Ma and from 1493 Ma to 1655 Ma, respectively) of these zircons greatly exceed the formation ages (mean of 853.7 ± 4.5 Ma), it can be suggested that parental magma of the granites may have remained settled in the crust for a long time after being generated from the partial melting of ancient materials.

5.c. Neoproterozoic magmatic events in North China Craton

Zircon U–Pb dating suggests that the gabbros (*c.* 835 Ma) and granites (*c.* 853 Ma) are contemporaneous. This provides evidence for the development of an early Neoproterozoic magmatic episode along the western margin of the NCC. In this region, there are several Neoproterozoic magmatic events whose ages are close to those of the Xiaosongshan complex. In the Qianlishan Mountains, there are many mafic dykes that are several metres wide and several kilometres long (Fig. 1b), consisting of diabase rocks. They are unconformably overlain by Carboniferous rocks and penetrate the Mesoproterozoic sediments. For one of the mafic dykes, a baddeleyite $^{207}Pb/^{206}Pb$ age of 813 Ma was determined (Peng, 2015; Peng *et al.* 2018). Li *et al.* (2004) reported the Jinchuan ultramafic intrusion with an age of ∼827 Ma in the adjacent Longshou Mountains, southwest of the Alxa Block. Peng *et al.* (2010) discovered Neoproterozoic Langshan acid volcanic rocks from the Mesoproterozoic Zha'ertaishan Group in the western margin of the NCC, which have an age of ∼810 Ma (Fig. 1a). Together with these ∼810 Ma and ∼827 Ma magmatic events, a few ∼837 Ma mafic dyke swarms in the Lanzhou–Qin'an area are also present (Liu *et al.* 2012). Nevertheless, additional work is necessary to further confirm the precise location of these dykes. Moreover, the Neoproterozoic (837–810 Ma) magmatic rocks not only exist in the western margin of the NCC, but also in the southern margin. Wang *et al.* (2011) examined the geochronology of gabbros, which were dated at *c.* 830 Ma by sensitive high-resolution ion microprobe (SHRIMP) and LA-ICP-MS methods, from the Luanchuan Group at the southern margin of the NCC. In conclusion, the coeval and chemically similar magmatic associations in the NCC and adjacent areas, such as the Alxa Block and Lanzhou–Qin'an area (Fig. 1b), suggest that these areas experienced *c.* 850–810 Ma magmatic activity during the Neoproterozoic.

Along with these 850–810 Ma magmatic events in the NCC, there are also several early Neoproterozoic dykes and/or sill swarms distributed in other parts of the NCC (Fig. 1a), such as the ∼925 Ma Dashigou dyke swarm, which comprises gabbro and diabase in the central NCC (Peng, 2011); the ∼900 Ma Sariwan sills, which are composed of dolerite, in the southeastern margin of the NCC (Peng *et al.* 2011b); the ∼925 Ma Dalian sills and dykes, which are composed of tholeiites and dolerites in the eastern NCC (Yang *et al.* 2004, 2007; Zhang *et al.* 2016); the 925–890 Ma Chulan sills and dykes, which also comprise mostly tholeiites and dolerites in the southeastern NCC (Liu *et al.* 2006; Wang *et al.* 2012); and the 900–830 Ma Zenghekou sills, which are composed of dolerites in the southern NCC (Wang *et al.* 2011). Moreover, similar *c.* 920 Ma magmatism also occurred in the Congo (Franssen & André, 1988; Tack *et al.* 2001) and São Francisco cratons (e.g. Correa-Gomes & Oliveira, 2000). On the basis of the precisely matched ages and similar chemical compositions, Peng *et al.* (2011a) proposed that the Bahia dykes in the

São Francisco craton and the Gangila–Mayumbian volcanics in the Congo craton could be the same large igneous provinces as the magmatic dykes/sills of the NCC. In summary, although the Neoproterozoic magmatic rocks were very weak in the NCC, the newly discovered Xiaosongshan complex, as well as these reported synchronous magmatic rocks in the NCC, indicate that the Neoproterozoic magmatic activity in the NCC could possibly have been stronger than what we identified before.

5.d. Implication for the relationship between the NCC and the Neoproterozoic supercontinent Rodinia

As discussed above, the Xiaosongshan magmatic rocks formed in the Neoproterozoic era, which was a critical period in the history of the Earth, were a witness to the waning stages of the break-up of the Rodinia supercontinent and the substantial migration of isolated cratons across a wide variety of latitudinal ranges during the assembly of Gondwana (Bowyer *et al.* 2017). Along with the drastic changes in Earth's crust, atmosphere and hydrosphere from Rodinia to Gondwana, the global tectonic framework was reorganized (Cawood *et al.* 2016; D. Li *et al.* 2018), resulting in a series of orogenies (Merdith *et al.* 2017). Magmatic events linked to the break-up of Rodinia are preserved in many continental fragments such as in Western Australia (e.g. Wingate & Giddings, 2000), the East European Craton (e.g. Nosova *et al.* 2008), India (e.g. Torsvik *et al.* 2001), Laurentia (e.g. Wingate, 2001), the northern Canadian Shield (e.g. Harlan *et al.* 2003), the Tarim Craton (e.g. Shu *et al.* 2011; Xu *et al.* 2013; Zhang *et al.* 2013; Wu *et al.* 2018) and South China (e.g. Zhou *et al.* 2002; ZX Li *et al.* 2003; WX Li *et al.* 2005; Dong *et al.* 2011; Cui *et al.* 2015). According to the Rodinia configuration (Hoffman, 1991), East Gondwanaland and Laurentia were located at a central position in the Rodinia supercontinent. Nevertheless, the precise locations of the South China Block and NCC during the Neoproterozoic era are controversial. Based on the study of tectonostratigraphy and palaeogeography, Li *et al.* (1996) suggested that the South China Block lay at the centre of the Rodinia supercontinent during the early Neoproterozoic.

In China, Neoproterozoic magmatic rocks, which might be related to the Rodinia supercontinent, are widespread in the South China Block and Tarim Craton, and some are distributed in the NCC. Therefore, fewer studies have dealt with the role of the NCC in the Rodinian reconstruction, and the question of whether the NCC was involved in the global Neoproterozoic magmatic events is still a mystery. Zhai *et al.* (2003) suggested that the NCC may have been located at a marginal position in Rodinia, and two metamorphic–magmatic events during ~1300–1000 Ma and ~850–650 Ma may exist in the NCC. Although these events were very weak, especially the latter, they are considered as indicators for the assembly and break-up of Rodinia. Hence, identifying the Neoproterozoic magmatic rocks in the NCC is critical to unravelling the Neoproterozoic history of the NCC and the relationship with other blocks and continents. The newly found Neoproterozoic magmatic rocks (Xiaosongshan complex) in the Helan Mountains, as well as the reported synchronous rocks in the southern margin (Wang *et al.* 2011), western margin (Li *et al.* 2004; Peng *et al.* 2010; Peng, 2015), eastern margin (Yang *et al.* 2004, 2007; Peng *et al.* 2011b; Zhang *et al.* 2016), southeastern margin (Liu *et al.* 2006; Peng *et al.* 2011b; Wang *et al.* 2012) and centre of the NCC (Peng, 2011), indicate that the NCC might have been connected with the Rodinia supercontinent during the Neoproterozoic. The newly discovered Neoproterozoic (*c.* 850 Ma) magmatic rocks

along the western margin of the NCC could be important for the Rodinian palaeogeographic reconstruction.

6. Conclusions

Based on the zircon U–Pb and Hf isotope compositions of the Xiaosongshan complex in the western margin of the NCC, we draw the following conclusions:

(1) LA-ICP-MC zircon U–Pb age dating of two representative samples (HL-39 and HL-30) yielded ^{206}Pb/^{238}U average ages of 835.5 ± 5.3 Ma and 853.7 ± 4.5 Ma, respectively, providing evidence for the development of early Neoproterozoic magmatic activity along the western margin of the NCC.

(2) *In situ* zircon Hf isotope compositions for the samples (HL-39 and HL-30) show that the εHf(*t*) values are 5.83–7.87 and −0.51 to 2.43, the corresponding Hf single-stage model ages (T_{DM1}) range from 1075 Ma to 1155 Ma and from 1348 Ma to 1461 Ma, respectively, and the Hf two-stage model ages (T_{DM2}) vary from 1176 Ma to 1289 Ma and from 1493 Ma to 1655 Ma, respectively. Viewed together, these data suggest that their parental magma formed by the reworking of the ancient crust evolved from Mesoproterozoic mantle.

(3) The newly found Neoproterozoic Xiaosongshan complex on the western margin of the NCC, as well as the reported Neoproterozoic magmatic rocks in other parts of the NCC, indicate that the NCC may have been connected with the supercontinent Rodinia during the Neoproterozoic.

Author ORCIDs. ⓘ jie Yang 0000-0002-9092-6346

References

Bouvier A, Vervoort JD and Patchett PJ (2008) The Lu–Hf and Sm–Nd isotopic composition of CHUR: constraints from unequilibrated chondrites and implications for the bulk composition of terrestrial planets. *Earth & Planetary Science Letters* **273**, 48–57.

Bowyer F, Wood RA and Poulton SW (2017) Controls on the evolution of Ediacaran metazoan ecosystems: a redox perspective. *Geobiology* **15**, 516–51.

Cawood PA, Strachan RA, Pisarevsky SA, Gladkochub DP and Murphy JB (2016) Linking collisional and accretionary orogens during Rodinia assembly and breakup: implications for models of supercontinent cycles. *Earth and Planetary Science Letters* **449**, 118–26.

Cherniak DJ, Hanchar JM and Watson EB (1997) Diffusion of tetravalent cations in zircon. *Contributions to Mineralogy & Petrology* **127**, 383–90.

Correa-Gomes LC and Oliveira EP (2000) Radiating 1.0 Ga mafic dyke swarms of Eastern Brazil and Western Africa: evidence of post-assembly extension in the Rodinia supercontinent? *Gondwana Research* **3**, 325–32.

Cui X, Jiang X, Wang J, Wang X, Zhuo J, Deng Q, Liao S, Wu H, Jiang Z and Wei Y (2015) Mid-Neoproterozoic diabase dykes from Xide in the western Yangtze Block, South China: new evidence for continental rifting related to the breakup of Rodinia supercontinent. *Precambrian Research* **268**, 339–56.

Dong XP, Hu JM, Li ZH, Zhao Y, Gong WB and Yang Y (2017) Provenance of Ediacaran (Sinian) sediments in the Helanshan area, North China Craton: constraints from U–Pb geochronology and Hf isotopes of detrital zircons. *Precambrian Research* **298**, 490–511.

Dong Y, Liu X, Santosh M, Zhang X, Chen Q, Yang C and Yang Z (2011) Neoproterozoic subduction tectonics of the northwestern Yangtze Block in South China: constraints from zircon U–Pb geochronology and geochemistry of mafic intrusions in the Hannan Massif. *Precambrian Research* **189**, 66–90.

Ernst RE, Bleeker W, Söderlund U and Kerr AC (2013) Large Igneous Provinces and supercontinents: toward completing the plate tectonic revolution. *Lithos* **174**, 1–14.

Ernst RE, Grosfils EB and Mège D (2001) Giant dike swarms: Earth, Venus, and Mars. *Annual Review of Earth & Planetary Sciences* **29**, 489–534.

Franssen L and André L (1988) The Zadinian Group (late Proterozoic, Zaire) and its bearing on the origin of the West-Congo orogenic belt. *Precambrian Research* **38**, 215–34.

Geng Y, Du L and Ren L (2012) Growth and reworking of the early Precambrian continental crust in the North China Craton: constraints from zircon Hf isotopes. *Gondwana Research* **21**, 517–29.

Geng Y and Zhou X (2010) Early Neoproterozoic granite events in Alax area of Inner Mongolia and their geological significance: evidence from geochronology. *Acta Petrologica et Mineralogica* **29**, 779–95 (in Chinese with English abstract).

Geng Y and Zhou X (2011) Characteristics of geochemistry and zircon Hf isotope of the Early Neoproterozoic granite in Alax area, Inner Mongolia. *Acta Petrologica Sinica* **27**, 897–908 (in Chinese with English abstract).

Greentree MR, Li ZX, Li XH and Wu H (2006) Late Mesoproterozoic to earliest Neoproterozoic basin record of the Sibao orogenesis in western South China and relationship to the assembly of Rodinia. *Precambrian Research* **151**, 79–100.

Griffin WL, Pearson NJ, Belousova E, Jackson SE, Achterbergh EV, O'Reilly SY and Shee SR (2000) The Hf isotope composition of cratonic mantle: LAM-MC-ICPMS analysis of zircon megacrysts in kimberlites. *Geochimica et Cosmochimica Acta* **64**, 133–47.

Halls HC, Campal N, Davis DW and Bossi J (2001) Magnetic studies and U–Pb geochronology of the Uruguayan dyke swarm, Rio de la Plata craton, Uruguay: paleomagnetic and economic implications. *Journal of South American Earth Sciences* **14**, 349–61.

Hanski E, Mertanen S, Rämö T and Vuollo J (2006) *Dyke Swarms – Time Markers of Crustal Evolution: Selected Papers of the Fifth International Dyke Conference in Finland, Rovaniemi, Finland, 31 July–3 Aug 2005 & Fourth International Dyke Conference, Kwazulu-Natal, South Africa 26–29 June 2001.* London: CRC Press.

Harlan SS, Heaman L, LeCheminant AN and Premo WR (2003) Gunbarrel mafic magmatic event: a key 780 Ma time marker for Rodinia plate reconstructions. *Geology* **31**, 1053–6.

Hawkesworth CJ and Kemp AIS (2006) The differentiation and rates of generation of the continental crust. *Chemical Geology* **226**, 134–43.

Hoffman PF (1991) Did the breakout of Laurentia turn Gondwanaland inside-out? *Science* **252**, 1409–12.

Hu Z, Gao S, Liu Y, Hu S, Chen H and Yuan H (2008a) Signal enhancement in laser ablation ICP-MS by addition of nitrogen in the central channel gas. *Journal of Analytical Atomic Spectrometry* **23**, 1093–101.

Hu Z, Liu Y, Gao S, Hu S, Dietiker R and Günther D (2008b) A local aerosol extraction strategy for the determination of the aerosol composition in laser ablation inductively coupled plasma mass spectrometry. *Journal of Analytical Atomic Spectrometry* **23**, 1192–203.

Hu Z, Liu Y, Gao S, Liu W, Zhang W, Tong X, Lin L, Zong K, Li M and Chen H (2012) Improved in situ Hf isotope ratio analysis of zircon using newly designed X skimmer cone and jet sample cone in combination with the addition of nitrogen by laser ablation multiple collector ICP-MS. *Journal of Analytical Atomic Spectrometry* **27**, 1391–9.

Isakson VH (2017) Geochronology of the Tectonic, Stratigraphic, and Magmatic Evolution of Neoproterozoic to Early Paleozoic, North American Cordillera and Cryogenian Glaciation. Boise State University Theses and Dissertations. 1262. doi: 10.18122/B2P42Z

Knudsen TL, Griffin W, Hartz E, Andresen A and Jackson S (2001) In-situ hafnium and lead isotope analyses of detrital zircons from the Devonian sedimentary basin of NE Greenland: a record of repeated crustal reworking. *Contributions to Mineralogy & Petrology* **141**, 83–94.

Kusky TM (2011) Geophysical and geological tests of tectonic models of the North China Craton. *Gondwana Research* **20**, 26–35.

Li D, Chen Y, Kang H, Xu B and Zhang Y (2018) Neoproterozoic continental arc system along the NW margin of Rodinia supercontinent: constraints from geochronological and geochemical studies of Neoproterozoic granitoids in the Diancangshan Massif. *Lithos* **316–317**, 77–91.

Li L, Zeng Z, Lu Y, Wei Y, Xiang S and Pan L (2014) LA-ICP-MS U-Pb geochronology of detrital zircons from the Zhaochigou Formation-complex in the Helan Mountain and its tectonic significance. *Science Bulletin* **59**, 1425–37.

Li W, Dong Y and Liu X (2018) Geochronology, geochemistry and Nd–Hf isotopes of the Xiaokouzi granite from the Helanshan complex: constraints on the Paleoproterozoic evolution of the Khondalite Belt, North China Craton. *Precambrian Research* **317**, 57–76.

Li WX, Li XH and Li ZX (2005) Neoproterozoic bimodal magmatism in the Cathaysia Block of South China and its tectonic significance. *Precambrian Research* **136**, 51–66.

Li X, Su L, Song B and Liu D (2004) SHRIMP U-Pb zircon age of the Jinchuan ultramafic intrusion and its geological significance. *Chinese Science Bulletin* **49**, 420–2.

Li ZX, Li XH, Kinny PD, Wang J, Zhang S and Zhou H (2003) Geochronology of Neoproterozoic syn-rift magmatism in the Yangtze Craton, South China and correlations with other continents: evidence for a mantle superplume that broke up Rodinia. *Precambrian Research* **122**, 85–109.

Li ZX, Zhang L and Powell CM (1996) Positions of the East Asian cratons in the Neoproterozoic supercontinent Rodinia. *Journal of the Geological Society of Australia* **43**, 593–604.

Liu DY, Nutman AP, Compston W, Wu JS and Shen QH (1992) Remnants of ≥3800 Ma crust in the Chinese part of the Sino-Korean craton. *Geology* **20**, 339–42.

Liu S, Hu R, Gao S, Feng C, Coulson IM, Feng G, Qi Y, Yang Y, Yang C and Tang L (2012) U–Pb zircon age, geochemical and Sr–Nd isotopic data as constraints on the petrogenesis and emplacement time of the Precambrian mafic dyke swarms in the North China Craton (NCC). *Lithos* **140–141**, 38–52.

Liu Y, Gao L, Liu Y, Song B and Wang Z (2006) Zircon U-Pb dating for the earliest Neoproterozoic mafic magmatism in the southern margin of the North China Block. *Chinese Science Bulletin* **51**, 2375–82.

Lu S, Li H, Zhang C and Niu G (2008) Geological and geochronological evidence for the Precambrian evolution of the Tarim Craton and surrounding continental fragments. *Precambrian Research* **160**, 94–107.

Lyons TW, Reinhard CT and Planavsky NJ (2014) The rise of oxygen in Earth's early ocean and atmosphere. *Nature* **506**, 307–15.

Merdith AS, Collins AS, Williams SE, Pisarevsky S, Foden JD, Archibald DB, Blades ML, Alessio BL, Armistead S, Plavsa D, Clark C and Müller RD (2017) A full-plate global reconstruction of the Neoproterozoic. *Gondwana Research* **50**, 84–134.

Nosova AA, Kuz'menkova OF, Veretennikov NV, Petrova LG and Levsky LK (2008) Neoproterozoic Volhynia-Brest magmatic province in the western East European craton: within-plate magmatism in an ancient suture zone. *Petrology* **16**, 105–35.

Nowell GM, Kempton PD, Noble SR, Fitton JG, Saunders AD, Mahoney JJ and Taylor RN (1998) High precision Hf isotope measurements of MORB and OIB by thermal ionisation mass spectrometry: insights into the depleted mantle. *Chemical Geology* **149**, 211–33.

Patchett PJ, Kouvo O, Hedge CE and Tatsumoto M (1982) Evolution of continental crust and mantle heterogeneity: evidence from Hf isotopes. *Contributions to Mineralogy & Petrology* **78**, 279–97.

Peng P (2011) Reconstruction and interpretation of giant mafic dyke swarms:a case study of 1.78 Ga magmatism in the North China craton. In *The Evolving Continents: Understanding Processes of Continental Growth* (eds TM Kusky, MG Zhai and WJ Xiao) pp. 163–78. Geological Society of London, Special Publication no. 338.

Peng P (2015) Precambrian mafic dyke swarms in the North China Craton and their geological implications. *Science China Earth Sciences* **58**, 649–75.

Peng P, Bleeker W, Ernst RE, Söderlund U and McNicoll V (2011a) U–Pb baddeleyite ages, distribution and geochemistry of 925 Ma mafic dykes

and 900 Ma sills in the North China craton: evidence for a Neoproterozoic mantle plume. *Lithos* **127**, 210–21.

Peng P, Wang XP, Zhou XT, Wang C, Sun FB, Su XD, Chen L, Guo JH and Zhai MG (2018) Identification of the similar to 810 Ma Qianlishan mafic dyke swarm and its implication for geological evolution of the western North China Craton. *Acta Petrologica Sinica* **34**, 1191–203.

Peng P, Zhai MG, Li Q, Wu F, Hou Q, Li Z, Li T and Zhang Y (2011b) Neoproterozoic (~900 Ma) Sariwon sills in North Korea: geochronology, geochemistry and implications for the evolution of the south-eastern margin of the North China Craton. *Gondwana Research* **20**, 243–54.

Peng R, Zhai Y, Wang J, Chen X, Liu Q, Lv J, Shi Y, Wang G, Li S, Wang L, Ma Y and Zhang P (2010) Discovery of Neoproterozoic acid volcanic rock in the western section of Langshan, Inner Mongolia, and its geological significance. *Chinese Science Bulletin* **55**, 2611–20 (in Chinese).

Scherer E, Münker C and Mezger K (2001) Calibration of the Lutetium-Hafnium Clock. *Science* **293**, 683–7.

Shu LS, Deng XL, Zhu WB, Ma DS and Xiao WJ (2011) Precambrian tectonic evolution of the Tarim Block, NW China: new geochronological insights from the Quruqtagh domain. *Journal of Asian Earth Sciences* **42**, 774–90.

Song B, Nutman AP, Liu D and Wu J (1996) 3800 to 2500 Ma crustal evolution in the Anshan area of Liaoning Province, northeastern China. *Precambrian Research* **78**, 79–94.

Srivastava RK (2010) *Dyke Swarms: Keys for Geodynamic Interpretation*. Berlin and Heidelberg: Springer.

Tack L, Wingate MTD, Liégeois JP, Fernandez-Alonso M and Deblond A (2001) Early Neoproterozoic magmatism (1000–910 Ma) of the Zadinian and Mayumbian Groups (Bas-Congo): onset of Rodinia rifting at the western edge of the Congo craton. *Precambrian Research* **110**, 277–306.

Torsvik TH, Carter LM, Ashwal LD, Bhushan SK, Pandit MK and Jamtveit B (2001) Rodinia refined or obscured: palaeomagnetism of the Malani igneous suite (NW India). *Precambrian Research* **108**, 319–33.

Trap P, Faure M, Lin W, Augier R and Fouassier A (2011) Syn-collisional channel flow and exhumation of Paleoproterozoic high pressure rocks in the Trans-North China Orogen: the critical role of partial-melting and orogenic bending. *Gondwana Research* **20**, 498–515.

Wang C, Bai S, Yang G, Lu Y, Jin X and Ma Z (2008) *The 1:250000 Regional Geological Survey Report of Jilantai (J48C001003)*. Yinchuan: Ningxia Hui Autonomous Region Monitoring Institute of Land and Resources Survey (in Chinese).

Wang QH, Yang DB and Xu WL (2012) Neoproterozoic basic magmatism in the southeast margin of North China Craton: evidence from whole-rock geochemistry, U-Pb and Hf isotopic study of zircons from diabase swarms in the Xuzhou-Huaibei area of China. *Science China Earth Sciences* **55**, 1461–79.

Wang X, Li X-P and Han Z-Z (2018) Zircon ages and geochemistry of amphibolitic rocks from the Paleoproterozoic Erdaowa Group in the Khondalite Belt, North China Craton and their tectonic implications. *Precambrian Research* **317**, 253–67.

Wang XL, Jiang SY, Dai BZ, Griffin WL, Dai MN and Yang YH (2011) Age, geochemistry and tectonic setting of the Neoproterozoic (ca 830 Ma) gabbros on the southern margin of the North China Craton. *Precambrian Research* **190**, 35–47.

Wingate MTD (2001) SHRIMP baddeleyite and zircon ages for an Umkondo dolerite sill, Nyanga Mountains, Eastern Zimbabwe. *South African Journal of Geology* **104**, 13–22.

Wingate MTD and Giddings JW (2000) Age and palaeomagnetism of the Mundine Well dyke swarm, Western Australia: implications for an Australia–Laurentia connection at 755 Ma. *Precambrian Research* **100**, 335–57.

Wu FY, Li XH, Zheng YF and Gao S (2007) Lu-Hf isotopic systematics and their applications in petrology. *Acta Petrologica Sinica* **23**, 185–220.

Wu G, Xiao Y, Bonin B, Ma D, Li X and Zhu G (2018) Ca. 850 Ma magmatic events in the Tarim Craton: age, geochemistry and implications for assembly of Rodinia supercontinent. *Precambrian Research* **305**, 489–503.

Wu Y and Zheng Y (2004) Genesis of zircon and its constraints on interpretation of U-Pb age. *Chinese Science Bulletin* **49**, 1554–69.

Xu Z-Q, He B-Z, Zhang C-L, Zhang J-X, Wang Z-M and Cai Z-H (2013) Tectonic framework and crustal evolution of the Precambrian basement of the Tarim Block in NW China: new geochronological evidence from deep drilling samples. *Precambrian Research* **235**, 150–62.

Yale LB and Carpenter SJ (1998) Large igneous provinces and giant dike swarms: proxies for supercontinent cyclicity and mantle convection. *Earth & Planetary Science Letters* **163**, 109–22.

Yang J, Wu F, Zhang Y, Zhang Q and Wilde S (2004) Identification of Mesoproterozoic zircons in a Triassic dolerite from the Liaodong Peninsula, Northeast China. *Chinese Science Bulletin* **49**, 1958–62.

Yang JH, Sun JF, Chen F, Wilde SA and Wu FY (2007) Sources and petrogenesis of Late Triassic dolerite dikes in the Liaodong Peninsula: implications for post-collisional lithosphere thinning of the Eastern North China Craton. *Journal of Petrology* **48**, 1973–97.

Yin C, Zhao G, Guo J, Sun M, Xia X, Zhou X and Liu C (2011) U–Pb and Hf isotopic study of zircons of the Helanshan Complex: constraints on the evolution of the Khondalite Belt in the Western Block of the North China Craton. *Lithos* **122**, 25–38.

Zhai M and Zhou Y (2015) General Precambrian geology in China. In *Precambrian Geology of China* (ed. M Zhai), pp. 3–16. Berlin and Heidelberg: Springer-Verlag

Zhai M, Shao JA, Hao J and Peng P (2003) Geological signature and possible position of the North China Block in the supercontinent Rodinia. *Gondwana Research* **6**, 171–83.

Zhang C-L, Zou H-B, Li H-K and Wang H-Y (2013) Tectonic framework and evolution of the Tarim Block in NW China. *Gondwana Research* **23**, 1306–15.

Zhang J, Zhao G, Sun M, Wilde SA, Li S and Liu S (2006) High-pressure mafic granulites in the Trans-North China Orogen: tectonic significance and age. *Gondwana Research* **9**, 349–62.

Zhang SH, Zhao Y, Ye H and Hu GH (2016) Early Neoproterozoic emplacement of the diabase sill swarms in the Liaodong Peninsula and pre-magmatic uplift of the southeastern North China Craton. *Precambrian Research* **272**, 203–25.

Zhao D (2003) Fabric analysis of olivine from Xiaosongshan Ultrabasic complexes. *Geology of Shaanxi* **21**, 45–8 (in Chinese with English abstract).

Zhao G and Cawood PA (2012) Precambrian geology of China. *Precambrian Research* **222**, 13–54.

Zhao G, Wilde SA, Cawood PA and Lu L (1998) Thermal evolution of Archean basement rocks from the eastern part of the North China Craton and its bearing on tectonic setting. *International Geology Review* **40**, 706–21.

Zhao G, Wilde SA, Cawood PA and Sun M (2001) Archean blocks and their boundaries in the North China Craton: lithological, geochemical, structural and P–T path constraints and tectonic evolution. *Precambrian Research* **107**, 45–73.

Zhao G, Sun M, Wilde SA and Li S (2005) Late Archean to Paleoproterozoic evolution of the North China Craton: key issues revisited. *Precambrian Research* **136**, 177–202.

Zhao G, Wilde SA, Guo J, Cawood PA, Sun M and Li X (2010) Single zircon grains record two Paleoproterozoic collisional events in the North China Craton. *Precambrian Research* **177**, 266–76.

Zhao G and Zhai M (2013) Lithotectonic elements of Precambrian basement in the North China Craton: review and tectonic implications. *Gondwana Research* **23**, 1207–40.

Zhou MF, Yan DP, Kennedy AK, Li Y and Ding J (2002) SHRIMP U–Pb zircon geochronological and geochemical evidence for Neoproterozoic arc-magmatism along the western margin of the Yangtze Block, South China. *Earth & Planetary Science Letters* **196**, 51–67.